Advances in Aircraft and Spacecraft Science, *Vol. 7, No. 1 (2020) 53-78*
DOI: https://doi.org/10.12989/aas.2020.7.1.053

How airplanes fly at power-off and full-power on rectilinear trajectories

Gilles Labonté*

Department of Mathematics and Computer Science,
Royal Military College of Canada, Kingston, Ontario, Canada

(Received October 24, 2018, Revised May 18, 2019, Accepted June 18, 2019)

Abstract. Automatic trajectory planning is an important task that will have to be performed by truly autonomous vehicles. The main method proposed, for unmanned airplanes to do this, consists in concatenating elementary segments of trajectories such as rectilinear, circular and helical segments. It is argued here that because these cannot be expected to all be flyable at a same constant speed, it is necessary to consider segments on which the airplane accelerates or decelerates. In order to preserve the planning advantages that result from having the speed constant, it is proposed to do all speed changes at maximum deceleration or acceleration, so that they are as brief as possible. The constraints on the load factor, the lift and the power required for the motion are derived. The equation of motion for such accelerated motions is solved numerically. New results are obtained concerning the value of the angle and the speed for which the longest distance and the longest duration glides happen, and then for which the steepest, the fastest and the most fuel economical climbs happen. The values obtained differ from those found in most airplane dynamics textbooks. Example of tables are produced that show how general speed changes can be effected efficiently; showing the time required for the changes, the horizontal distance traveled and the amount of fuel required. The results obtained apply to all internal combustion engine-propeller driven airplanes.

Keywords: airplane accelerated trajectory; inclined rectilinear motion, airplane equation of motion; automatic trajectory planning; gliding; climbing

1. Introduction

This article presents a contribution to the project of endowing unmanned aerial vehicles (UAVs) with complete autonomy. A fundamental ability that this requires is for the UAV to generate by itself alternative trajectories to reach its goal, when unforeseen circumstances occur that force it to deviate from its original flight plan.

The first studies on 3D trajectory planning were mainly concerned with finding the shortest path between two points, with specified departure and arrival directions, as initiated by Dubins (1957). However, today, trajectories are optimized with respect to many other factors such as the amount of fuel used, the altitude, the avoidance of detection, of danger and of forbidden zones, and the dynamical abilities of the UAV itself. A good overview of the factors to consider was given by Roberge *et al.* (2012).

*Corresponding author, Emeritus Professor, E-mail: gilles.labonte@rmc.ca

http://www.techno-press.org/?journal=aas&subpage=7 ISSN: 2287-528X (Print), 2287-5271 (Online)

1.1 Building up trajectories with motion primitives

An efficient method for automatically constructing trajectories has been proposed by Frazzoli *et al.* (2005). It consists in concatenating elementary trajectory segments, called motion primitives, for which the properties are calculated in advance and stored in an on-board library. The motion primitives usually considered are rectilinear, circular and helical segments.

A particular, very often used, realization of this approach consists in starting by building a skeleton trajectory of connected rectilinear segments, and then smoothing out the connections, in order for the velocity to be continuous. This smoothing can be done with splines, as do Judd (2001), Zheng *et al.* (2003), Nikolos *et al.* (2003), Yang and Sukkarieh (2010), Jiabo *et al.* (2012) and Wang *et al.* (2017). It can also be done with arcs of circles as do Dubins (1957), Chandler *et al.* (2000), Jia and Vagners (2004), Chitsaz and LaValle (2007), Hwangbo *et al.* (2007), Allaire *et al.* (2009), Xia *et al.* (2009), Ambrosino *et al.* (2009), Babaei and Mortazavi (2010), Hota and Ghose (2010, 2014), Roberge *et al.* (2012), Niendorf *et al.* (2013), Gao *et al.* (2013), Zhan *et al.* (2014), Wang *et al.* (2014), Rudnick-Cohen *et al.* (2015), Ramana *et al.* (2016), Kok and Rajendran (2016). Actually, smoothing with arcs of circles is far preferable to smoothing with splines because the flyability of the resulting trajectory is more readily analyzed.

Many of the studies mentioned above, actually construct a path instead of a trajectory, because they only specify the spatial curve that the airplane should follow and do not specify the speed at which it should fly it. This is not sufficient because essentially all realistic trajectory optimization criteria require the knowledge of the speed of the UAV. It is interesting to note that in studies that include the speed, essentially all the authors take it to be constant on the whole trajectory. This consideration simplifies the calculations, however, trajectories flown at constant speed are not expected to be optimal in general. For example, if the travel time should be as small as possible, then some segments of the trajectory should definitely be traveled faster than others, if they can. Furthermore, the speed at which a segment can be flown depends very much on its inclination and its altitude, as was discussed in Labonté (2016, 2019). For example, a Silver Fox-like UAV can only fly at constant speed on a rectilinear trajectory inclined at 5^0 with speeds between 15.8 and 52.7 m/s, while if the rectilinear trajectory is inclined at -10^0, its constant speed must be between 54.9 and 63.4 m/s (Labonté 2018). There is then no common speed at which these two rectilinear segments can be flown. It will in fact generally be difficult, if at all possible, to find a single speed at which all the segments of the trajectory can be flown.

These facts provide a strong motivation for the present work in which we propose to include as motion primitives, rectilinear segments on which the airplane accelerates or decelerates. Accelerations and decelerations will be considered to be as short as possible, in order for the major part of the segment to be subsequently traveled at constant speed. This means that we will consider accelerations performed at full-power and decelerations at power-off.

1.2 Airplane model

Essentially all studies of airplane trajectory planning, except for Roberge *et al.* (2012), adopt the airplane model of Dubins (1957), according to which the airplane flies at constant speed, while respecting constant bounds on the vertical component of the velocity and on the turning radius. However, these bounds are never constant: they depend very strongly on the altitude and on the inclination of the trajectory (Labonté 2018). The present work does take into account the most important constraints imposed by the airplane dynamics; it uses the realistic airplane model

described by Anderson (2000) and Stengel (2004). It also uses the same nomenclature.

The application of the formulas derived in this study is illustrated with airplanes that have similar properties as the following two different familiar airplanes:

- the Cessna 182 Skylane, which has a reciprocating engine with a constant speed propeller,
- a Silver Fox-like unmanned aerial vehicle (UAV) which has a reciprocating engine with a fixed pitch propeller.

The characteristics we have used for these airplanes are listed in Appendix A.

1.3 Dynamics of airplanes on inclined trajectories

The motion of airplanes on rectilinear trajectories is discussed essentially in all textbooks on airplane dynamics. However, we did not find any that provides a complete solution to the descending or the climbing flight equations that describes the whole trajectory. Instead, only instantaneous gliding and climbing rates are calculated, which are assumed to hold for the whole trajectory. This local calculation is then used to derive the optimal distance and duration of the manoeuvre (Torenbeek 1976, Hale 1984, Mair and Birdsall 1992, Anderson 2000, Eshelby 2000, Yechout *et al.* 2003, Stengel 2004, Filippone 2006 and Boschetti *et al.* 2015). An important shortcoming of these calculations is that they consider the air density, the temperature and the airplane weight to be constant. The inadequacy of this approach, when longer trajectories are considered, is recognized and explicitly stated by Anderson (2000), Eshelby (2000), Stengel (2004) and Filippone (2006).

Furthermore, when optimal gliding and climbing are discussed in textbooks, the trajectories are considered to be inclined at angles θ that are small so that $\cos(\theta) \approx 1$. This may be justified for most commercial airplanes, for which θ is at most about 10^0-15^0, but it is not true for UAVs and fighter airplanes that can fly much bolder manoeuvres.

It is our purpose in the present article to examine flights at any angle of inclination. We shall take into account the variations of the air density along the trajectory and of the weight of the airplane due to fuel burn. We shall determine the actual parameters with which optimal glides and climbs occur over trajectories of any length. We shall also present examples of calculations for our two different sample airplanes. We construct example of tables that exhibit the properties of maximum decelerations and accelerations. These tables show the speeds attainable, the time required, the horizontal distance flown, and the amount of fuel required. These are the quantities of outmost interest for the process of planning of optimal flights (Mair and Birdsall 1992).

The analysis presented in this article does not take into account the perturbations of the atmosphere. As in Phillips (2004), the material we present should be seen as a preliminary study of airplane performance. The results presented are otherwise quite general and constitute important tools not only for UAV trajectory planning, but also for the analysis of the motion of all propeller driven airplanes.

1.4 Organization of the article

We start by recalling the description of the position, velocity and acceleration of an airplane on a rectilinear trajectory, according to the Newton equation of motion, while taking into account the variation of the airplane mass due to fuel burn. We derive the equations that correspond to the constraints on the load factor, the lift coefficient and the power available.

We examine the standard textbook analysis of the glides at power-off, for the longest horizontal

distance and for the longest duration. We also examine the textbook optimal climbs at full power, in particular the steepest and the fastest climbs. While textbooks normally consider only small angle of inclination of the trajectory, we extend this analysis in order to cover all values of that angle.

We then solve the equation of motion for power-off and full power situations, with the help of the Runge-Kutta algorithm of order 4, at 10 digit precision. This allows us to determine the actual parameters for which the optimal glides and climbs occur. We produce graphs that illustrate how the speed, the altitude and the acceleration of the airplane vary in the optimal glides and climbs.

Finally, we give examples of tables that list the characteristics of power-off and full-power trajectories. We propose an algebraic expression to describe the speed, the altitude and the acceleration on such trajectories.

2. Accelerated motion on rectilinear trajectories

Let us consider an airplane that flies at a speed that varies in time $V_\infty(t)$, on a rectilinear segment, which extends from the point $\boldsymbol{x}_i$ to the point $\boldsymbol{x}_f$. In order to simplify the notation, we place the coordinate system such that the z-axis is vertical, the rectilinear segment lies in the x-z plane, with $\boldsymbol{x}_i$ on the z-axis, at the altitude h_i, and such that $\boldsymbol{x}_f$ has a positive x-coordinate. The position of the center of mass $\boldsymbol{x}(t)$ of the airplane is then given by:

$$\mathbf{x}(t)=[0,0,h_i]+d(t)\boldsymbol{\tau} \quad \text{with} \quad \boldsymbol{\tau}=[\cos(\theta),0,\sin(\theta)],$$

in which θ is the angle that the trajectory makes with the horizontal x-y plane, $\boldsymbol{\tau}$ is the unit tangent vector to the trajectory and d is the distance traveled. d is a positive definite, monotonically increasing function of t, such that $d(0)=0$. If the trajectory is ascending, $\theta > 0$, and if it is non-ascending, $\theta \le 0$. In all cases, $0 \le |\theta| \le \pi/2$. The velocity on this trajectory is

$$\mathbf{v}(t)=V_\infty \boldsymbol{\tau} \quad \text{with} \quad V_\infty = d'(t).$$

The acceleration is $\alpha(t)\boldsymbol{\tau}$ with $\alpha(t)=V_\infty'(t)$. In the present study, we consider that the speed changes as fast as possible from one value to another one, therefore, the acceleration will keep the same sign at all times when it is not null.

Labonté (2012) gave the form of Newton's equation of motion, for an airplane on a rectilinear inclined trajectory, which takes into account the variation of the mass of the airplane due to fuel consumption. Its normal and longitudinal components are respectively:

$$L = W\cos(\theta) \tag{1}$$

$$\frac{W}{g}\left[\frac{dV_\infty}{dt}\right]-\frac{AFR}{g}\left[\frac{dW}{dt}\right]V_\infty = T_R - D - W\sin(\theta), \tag{2}$$

in which L is the lift, W is the weight of the airplane, "AFR" is the air to fuel ratio for the combustion engine, T_R is the thrust required for the motion and D is the drag. The right-hand side (RHS) of Eq. (2) is the sum of the forces that act in the direction of the motion.

2.1 Load factor

Eq. (1) yields the value of the load factor n as:

$$n = \frac{L}{W} = cos(\theta)$$

.

The integrity of the airplane structure requires that its value be bounded at all times, such that

$$n_{min} \leq n \leq n_{max}.$$

Since here n is always non-negative, this inequality implies

$$cos(\theta) \leq n_{max}.$$

For most airplanes, this condition is satisfied for all θ since usually $n_{max} > 1$.

2.2 Lift coefficient

Upon replacing L by its expression from Eq. (1), one obtains

$$C_L = \frac{2W\,cos(\theta)}{\rho_\infty S V_\infty^2} \quad . \tag{3}$$

Thus, the lift coefficient C_L changes in time because W, ρ_∞ and V_∞ do. However, it must always satisfy the constraint

$$C_L \leq C_{Lmax}. \tag{4}$$

Ineqs. (3) and (4) imply a lower bound V_{LB} for the speed:

$$V_\infty(t) \geq V_{LB} \qquad \text{with} \qquad V_{LB} = \sqrt{\frac{2W\,cos(\theta)}{\rho_\infty S C_{L\,max}}} \quad . \tag{5}$$

If its speed goes below V_{LB}, the airplane will stall because the lift is too small to keep it flying on the prescribed trajectory.

2.3 Power

When an internal combustion engine produces the power P_P that is transferred to a propeller of efficiency η, the power available to move the airplane P_A is: $P_A = \eta P_P$ (Anderson 2000). The rate of fuel usage, when this power is produced, is:

$$\frac{dW}{dt} = -c\,P_P = -\frac{c}{\eta} P_A \tag{6}$$

in which c is the specific fuel consumption and η is the propeller efficiency. At the altitude h, the maximum power available is

$$P_{Amax}(h) = \eta\, P_{P\,max}(h) = \eta \frac{\rho_\infty(h)}{\rho_\infty(0)} P_{P\,max}(0)$$

.

where $P_{Pmax}(0)$ is the maximum power that the engine can produce at sea level.

3. Textbook description of optimal glides

The "Gliding Flight" section of textbooks considers an airplane that flies at power-off, with constant speed, on a rectilinear trajectory inclined at an angle θ with the horizon. Thus $T_R = 0$, and since no fuel is consumed $dW/dt = 0$ and, the speed being constant, $dV_\infty/dt = 0$. The equation of motion Eq. (2) then becomes simply

$$D + W\sin(\theta) = 0 ,$$

which with Eq. (1) implies

$$\tan(\theta) = -\frac{1}{L/D} = -\frac{C_D}{C_L} . \tag{7}$$

3.1 Largest horizontal distance glide

The geometry of the trajectory implies that the longest horizontal distance traveled in a glide is obtained when θ has its smallest possible value. Upon differentiating $\tan(\theta)$ with respect to C_L, it is found that the minimum of θ occurs when $C_L = C_{Ldg} = \sqrt{\pi e A R C_{D0}}$, for which value the angle is θ_{dg} such that

$$\tan(\theta_{dg}) = 2\sqrt{\kappa C_{D0}} , \text{ with } \kappa = (\pi e A R)^{-1} . \tag{8}$$

For this value for the angle and the lift coefficient, Eq. (3) yields the speed

$$V_{dg} = \sqrt{\frac{2W}{\rho_\infty S}}\left[\pi e A R C_{D0} + 4C_{D0}^2\right]^{-1/4} . \tag{9}$$

It is worth noting that the optimal lift coefficient C_{Ldg} is independent of the altitude so that the angle of descend θ_{dg} is the same at all altitudes. However this analysis has a shortcoming in that the glide speed V_{dg} depends on the air density and therefore cannot really remain constant, in contradiction to the initial hypothesis. This fact is often pointed out as in Example 6.9 of Anderson (2000). We illustrate it in Table 1 that shows sample values of V_{dg} for Silver Fox-like UAV and the Cessna 182 at various altitudes.

Table 1 Standard longest distance glide parameters for two different airplanes

Silver Fox-like UAV	$\theta_{dg} = -4.17^0$	Cessna 182,	$\theta_{dg} = -4.63^0$
Altitude (m)	V_{dg} (m/s)	Altitude (m)	V_{dg} (m/s)
1000	22.42	1000	41.49
2000	23.56	3000	45.87
3000	24.78	5000	50.95

3.2 Endurance (longest duration) glide

The vertical speed is $h' = V_\infty \sin(\theta)$. Eqs. (1) and (7) imply

$$h' = -\sqrt{\frac{2W}{\rho_\infty S}} \frac{C_D}{\left(C_L^2 + C_D^2\right)^{3/4}} .$$

The time required to descend is longest when h' is maximum. There are five critical points at which the derivative of h' with respect to C_L is null, there is only one of them that corresponds to the absolute maximum for h'. It is

$$C_{Leg} = \frac{1}{2\kappa}\left\{\left(1 - 4\kappa C_{D0}\right) - \sqrt{1 - 32\kappa C_{D0}}\right\}^{1/2} . \tag{10}$$

Eq. (7) yields the angle for the longest duration glide θ_{eg} when $C_L = C_{Leg}$ and $C_D = C_{Deg}$, with $C_{Deg} = C_{D0} + \kappa C^2_{Leg}$. Eq. (3) then yields for the speed

$$V_{eg} = \sqrt{\frac{2\cos(\theta_{eg})W}{\rho_\infty C_{Leg} S}} . \tag{11}$$

Example of values are:

For the Silver Fox-like UAV, θ_{eg} = -4.83^0 and V_{dg} = 18.75 m/s at an altitude of 3000 m.

For the Cessna 182, θ_{eg} = -5.36^0 and V_{eg} = 38.52 m/s at an altitude of 5000 m.

As was the case for the longest distance glide, the optimal lift coefficient C_{Leg} and angle of descend θ_{eg} are altitude independent. This analysis of the endurance glide has the same shortcoming as that of the longest distance glide, in that it considers the speed V_{eg} to be constant while it neglects the variation of air density with altitude.

4. Textbook description of optimal climbs

The "Climbing Flight" section of textbooks discuss the flight of an airplane at full power, with constant speed, on a rectilinear trajectory inclined at a positive angle θ with the horizon. They neglect fuel consumption so that the equation of motion Eq. (2) reduces to

$$T_R - D - W\sin(\theta) = 0 , \tag{12}$$

which with Eq. (1) implies

$$\tan(\theta) = \frac{T_R - D}{L} . \tag{13}$$

As with gliding, two situations are considered of particular interest, namely the steepest climbs and the fastest climbs. The determination of the value of the angle θ at which this occurs is more involved than it was for the gliding motion due to the fact that the variables C_L, V_∞ and θ that appear on the RHS of Eq. (17) are all inter-related. Because of this, in all textbooks that we have consulted, only small angles are considered, for which $\cos(\theta) \approx 1$. It is however possible, at the cost of more elaborate calculations, to deal with angles θ that could take any value. This is what we shall do hereafter.

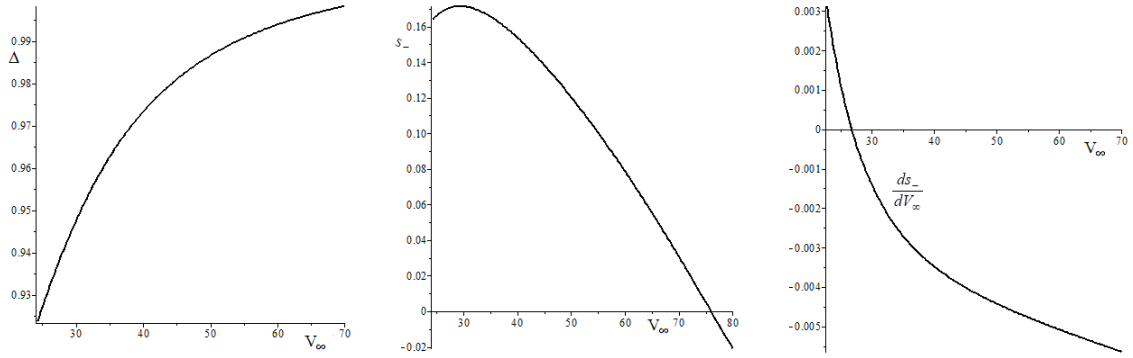

(a) Discriminant factor Δ (b) $s\_(V_\infty)$ (c) Derivative of $s\_(V_\infty)$

Fig. 1 Δ, s- and its derivative in terms of V_∞ for the Cessna 182

Since $P_R=V_\infty T_R$, the maximum thrust available at speed V_∞ is $T_{Amax}=\frac{P_{Amax}}{V_\infty}$. Upon substituting the value of C_L from Eq. (3) into Eq. (12), the latter equation becomes

$$\frac{\eta\,\rho_\infty(h)P_{Pmax}(0)}{V_\infty\rho_s}-\rho_\infty V_\infty^2\alpha_1+\frac{2\kappa W^2(s^2-1)}{\rho_\infty S V_\infty^2}-Ws=0 \tag{14}$$

with

$$\alpha_1=\frac{S\,C_{D0}}{2} \qquad \text{and} \qquad s=sin(\theta)\,.$$

At this point, textbooks use the small angle hypothesis, $\cos(\theta)\approx 1$ so that the third term on the LHS of the equation can be neglected. This greatly simplifies the analysis because Eq. (14) is then simply linear in s. Without this small angle hypothesis, Eq. (14) is a quadratic equation for s that corresponds to an upward concave parabola. If this equation does not have real roots, then the LHS of Eq. (14) would always be positive. Since Eq. (14) is the same as Eq. (12), written out explicitly, the fact that LHS is always positive, means that the thrust is always larger than the drag and the component of the weight along the trajectory. This happens when the thrust provided is so large that there would be no angle θ for which Eq. (12) can hold. In such a situation, the airplane would necessarily accelerate, i.e., the speed and the angle of climb could not be constant, contrary to the hypotheses made. For the motion considered to be possible, it is therefore necessary for Eq. (14) to have real roots, which requires that its discriminant $W\Delta$ be non-negative, with

$$\Delta=1+\frac{8\kappa}{S}\left[\alpha_1+\frac{2\kappa\tilde{W}^2}{SV_\infty^4}-\frac{\eta P_{Pmax}(0)}{\rho_s V_\infty^3}\right] \quad \text{in which} \quad \tilde{W}=\frac{W}{\rho_\infty}\,.$$

Δ is dimensionless and Fig. 1(a) shows how it varies with V_∞ for the Cessna 182. It can be demonstrated that for this airplane, as well as for the Silver Fox-like UAV, it is always positive. Eq. (14) then has the following two real solutions

$$s_{\pm} = \frac{SV_{\infty}^2}{4\kappa\tilde{W}}\left[W \pm \sqrt{\Delta}\right].$$

The solution s_+ is larger than 1 so that it cannot be a value of $sin(\theta)$ and therefore, only the solution s_- should be considered. Fig. 1(b) shows how s_- varies with V_∞ for the Cessna 182. For the Silver Fox-like UAV, the curve for the parameters Δ and s_- are very similar, except that s_- does not have a local maximum.

4.1 Steepest climb

The steepest climb occurs when θ is maximum, i.e., when s_- is maximum. This maximum occurs at the speed usually denoted by V_Y. This maximum occurs either at the end of the domain of V_∞ or at a critical point at which the derivative of s_- with respect to V_∞ is null. Recall that, in the standard discussions found in textbooks, the air density is considered constant so that the derivative of s_- is

$$\frac{ds_-}{dV_\infty} = \frac{kV_\infty}{2\tilde{W}}\left[1 - \sqrt{\Delta}\right] - \frac{kV_\infty^2}{8\tilde{W}\sqrt{\Delta}}\left[\frac{d\Delta}{dV_\infty}\right],$$

with

$$\frac{d\Delta}{dV_\infty} = -\frac{8}{kV_\infty^3}\left\{\frac{8\tilde{W}^2}{kV_\infty^2} + \frac{P_{Pmax}(0)}{\rho_s}\left[\frac{d\eta}{dV_\infty} - \frac{3\eta}{V_\infty}\right]\right\}.$$

A representation for η is clearly required for the study of the derivative of s_-. Fig. 1(c) shows how the derivative of s_- varies with V_∞ for the Cessna 182.

For this airplane that starts at sea level, V_Y =26.83 m/s, the angle of ascension is 11.92^0 and the ascension rate is 5.54 m/s.

For the Silver Fox-like UAV, the variable s_- is monotonically decreasing so that its maximum occurs at the minimum possible value of V_∞ for which the constraint of Ineq. (5) is respected. This speed is V_Y = 11.57 m/s. The angle of ascension is then 57.61^0 and the ascension rate is 9.77 m/s.

4.2 Fastest climb

The fastest climb rate is the maximum value of $h' = V_\infty sin(\theta) = V_\infty s_-(V_\infty)$. In order to determine this value, the derivative of h' with respect to V_∞ has to be examined. This derivative is

$$\frac{dh'}{dV_\infty} = s_-(V_\infty) + V_\infty\left[\frac{ds_-}{dV_\infty}\right].$$

Figs. 2(a) and 2(b) show respectively how h' and its derivative vary with V_∞, for the Cessna 182, at sea level.

For this airplane, h' is maximum at the speed denoted V_X that is V_X = 43.23 m/s. The climb

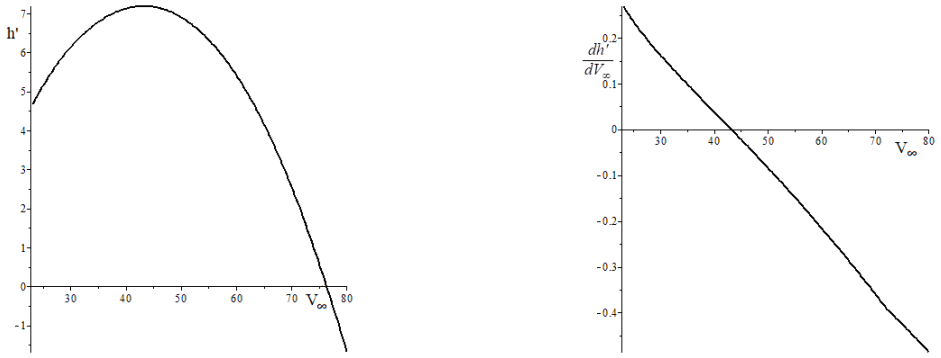

(a) Climb rate (b) Derivative of climb rate

Fig. 2 Climb rate and its derivative as functions of V_∞ for the Cessna 182

angle is then 9.57^0 and the climb rate is 7.18 m/s.

For the Silver Fox-like UAV, h' is maximum at V_X = 34.92 m/s. The climb angle is 32.91^0, and the climb rate is 18.97 m/s.

4.3 Remark

The above analysis of optimal climbs has two shortcomings. The first one is the same one as was mentioned for the optimal glides textbook analysis, namely that the speed V_∞ cannot, in fact, be constant because all the equations used in the derivation contain the air density which changes with the altitude. The second one is that the weight of the airplane also cannot be considered to remain constant on long climbs since climbing at full power requires an appreciable amount of fuel. We shall hereafter exhibit the extent of these shortcomings, when we examine the actual solutions to the equation of motion.

5. Exact description of optimal glides

When the airplane is moving at power-off, no fuel is used so that its weight is constant, and Eq. (2) reduces to

$$\frac{W}{g} a_{min} = -D - W\,sin(\theta) \quad , \tag{15}$$

in which a_{min} denotes the smallest acceleration possible. Upon replacing D by its value in this equation, it becomes

$$a_{min} = -g\left\{ sin(\theta) + \frac{\alpha_1}{W}\rho_\infty V_\infty^2 + \frac{\delta_1 W}{\rho_\infty V_\infty^2} \right\} \quad , \qquad \text{with} \qquad \delta_1 = \frac{2\,cos^2(\theta)}{\pi\, e\, AR\, S} \tag{16}$$

Since, as mentioned above, there does not exist constant speed solutions, we shall determine the parameters for which gliding is optimal by solving the equation of motion

$$\frac{dV_\infty}{dt} = a_{min}(V_\infty) \quad . \tag{17}$$

Since we could not find an exact solution to this differential equation, we solved it numerically with the help of well-established numerical methods. Thus, we have used the function "dsolve" from the mathematical software Maple (Maplesoft 2018), which implements a Runge-Kutta algorithm of order 4, to obtain numerical solutions that are valid to 10 digits.

5.1 Slowest and longest glides

In order to determine the angle and speed for which the glides are optimal, we solved Eq. (17) for many different angles and all speeds for which the glide was possible, at each 0.1 m/s intervals. We plot the glide duration for each solution calculated. A pattern is then clearly seen to emerge in these graphs, which points out the best angle and speed for the glides. These calculations were performed for both of the sample airplanes that we consider.

For the Silver Fox-like UAV, we considered glides that start at 1800 m and for the Cessna 182, glides that start at 2700 m. In both cases, the airplane glided until it reached sea level. We note that there was no particular reason to select these starting altitudes, other than that they are not extreme, being about half way to the service ceiling of the airplane.

Fig. 3(a) shows the graph of the duration of the glides for various angles of inclination for the Silver Fox-like UAV. The longest duration glide is seen to occur at the glide angle θ_{og} with θ_{og} = 0.997 θ_{dg}; at this angle, the glide lasts for 1146.0 s (19 min and 6 s) and the horizontal distance covered is *24,738.1* m. Furthermore, it was determined that the smallest initial speed yielded the longest duration glide. The longest horizontal distance will also be covered at the same angle θ_{og}, because this is the smallest angle for which the motion is possible. The longest range glide at θ_{og}, is obtained with the initial speed V_{og} = 23.21 m/s, and the final speed will be 14.18 m/s.

Fig. 3(b) shows the corresponding glide duration graph for the Cessna 182. The longest duration glide occurs at the glide angle θ_{og} which is 0.99 θ_{dg}; its duration is 853.1 s (4 min and 13.1 s). Again, the smallest initial speed yielded the longest duration glide. The largest horizontal distance possibly covered is 33,691.0 m, which occurs also with the same angle θ_{og}. For the largest range glide the initial speed is V_{og} =44.3 m/s, and the final speed is 23.30 m/s.

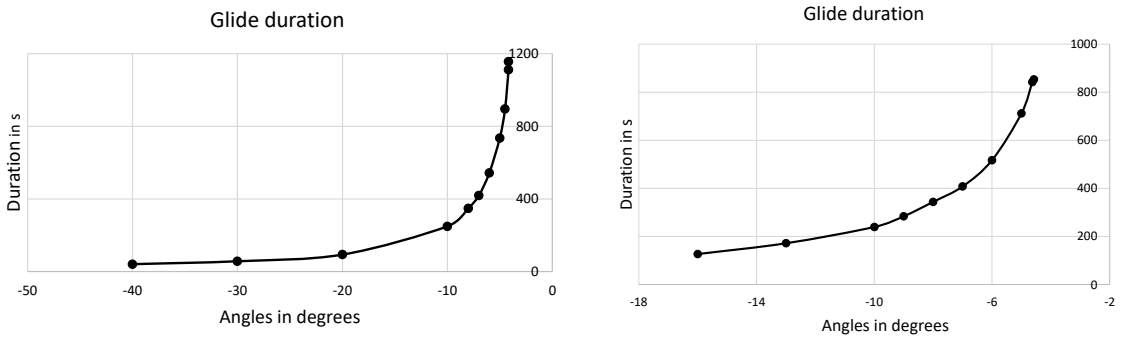

(a) For the Silver Fox-like UAV (b) For the Cessna 182

Fig. 3 Glide duration at various angles

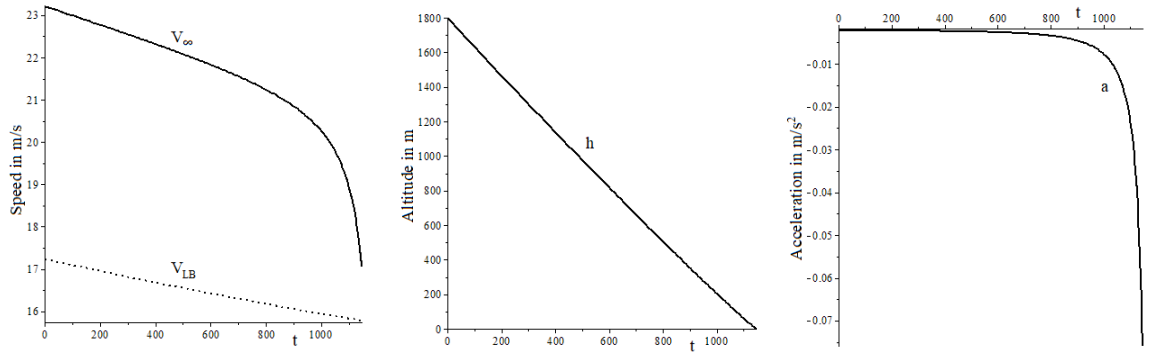

(a) Speed (b) Altitude (c) Acceleration

Fig. 4 Speed, altitude and acceleration as functions of t, for the Silver Fox-like UAV at power-off, from 1800 m to sea level, with the optimal glide parameters

Fig. 4 illustrates the behavior of the speed, altitude and acceleration, in the longest range solution. In Fig. 4(a), the speed V_∞ is shown together with the stall speed V_{LB}, which is represented by the dotted line. The glide speed is not constant: it decreases all through the flight due to the increase in the air density. Its decrease appears to be regular for most of the trajectory but it precipitates sharply at the end of the glide. The airplane reached sea level just before its speed decrease to the value of the stall speed. From this behavior, we conclude that the actual optimal initial speed for the glide will be obtained with conditions for which the airplane attains its stall speed right at the time it reaches the ground. As Fig. 4(b) shows, the altitude h(t) decreases almost linearly, so that the speed could be approximated by some constant, although it is not clear how its value could theoretically be determined. Fig 4(c) shows the acceleration as function of time. It is very small, almost null, for most of the glide and it suddenly decreases as the airplane approaches its stall speed.

The corresponding graphs for the speed, the altitude and the acceleration for the Cessna 182 have very much the same appearance as those for the Silver Fox-like UAV, shown in Fig. 4.

For both airplanes, all the trajectories that are less inclined than the optimal angle θ_{og} lead to a stall before the airplane reaches sea level.

6. Exact description of optimal climbs

In the present section, we determine the actual parameters that yield the steepest and the fastest climbs. We do so by examining the solutions of the equation of motion when the airplane is flying at full-power, while taking into account the variation of air density with the altitude and the variation of the airplane weight due to fuel burning. At full-power, the power required for the motion is $P_R = P_{Amax}$ and Eq. (6) becomes

$$\frac{dW}{dt} = -cP_{Pmax}(h) = -\frac{c}{\eta}P_{Amax}(h) = -\frac{c\rho_\infty(h)}{\eta\rho_\infty(0)}P_{Amax}(0)\,. \tag{18}$$

Eqs. (2) and (6) yield for the maximum acceleration

$$a_{max} = -g\left\{ sin(\theta) + \frac{\alpha_1}{W}\rho_\infty V_\infty^2 + \frac{\delta_1 W}{\rho_\infty V_\infty^2} - G(V_\infty)\frac{\rho_\infty P_{Pmax}(0)}{\rho_s W}\right\}, \tag{19}$$

in which

$$G(V_\infty) = \frac{\eta(V_\infty)}{V_\infty} - \frac{c(AFR)V_\infty}{g}.$$

The equation of motion is then

$$\frac{dV_\infty}{dt} = a_{max}(V_\infty). \tag{20}$$

The amount of fuel used during the acceleration is obtained by solving Eq. (18). For both the Silver Fox-like UAV and the Cessna 182, the climbs considered started at sea level. The parameters that yield the optimal climbs were determined by solving the equation of motion at various angles for many different speeds and plotting the climb durations. A clear pattern emerges in these graphs that points out the value of the parameters for the optimal climbs.

6.1 Climb duration vs speed

We endeavored to determine the actual optimal climb speed by analyzing how our sample two airplanes climb from sea level to various altitudes. Here are typical results obtained with the Silver Fox-like UAV climbing up to the altitude of 1800 m and the Cessna 182 to 2700 m, which are altitudes that are about halfway to their service ceiling. These results are quite typical of what is observed at any angle of inclination for both our sample airplanes.

The duration of the climbs of the Silver Fox-like UAV at 30^0 with various speeds is shown in the graph of Fig. 5(a). The corresponding behavior for the climbs of the Cessna 182 at 7.5^0 is shown in the graph of Fig. 5(b). As can be observed, for both airplanes, at any angle of climb, the shortest climb duration occurs at the maximum possible speed.

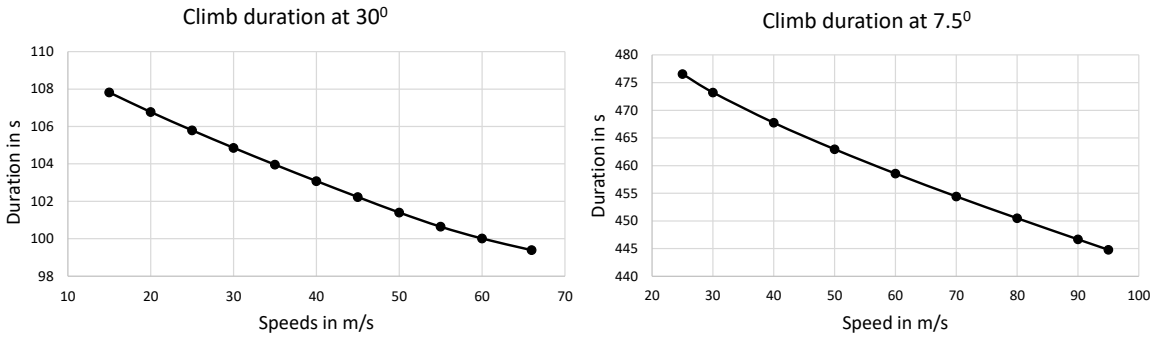

(a) For the Silver Fox-like UAV up to 1800 m (b) For the Cessna 182 up to 2700 m

Fig. 5 Climb duration in terms of the speed

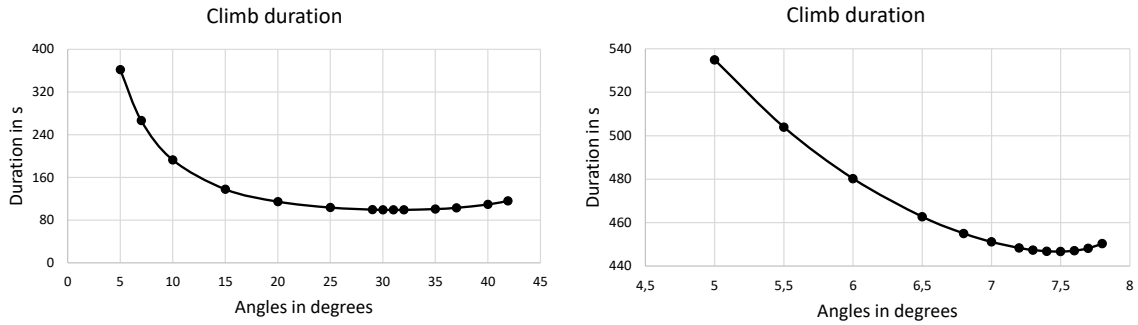

(a) For the Silver Fox-like UAV up to 1800 m (b) For the Cessna 182 up to 2700 m

Fig. 6 Climb duration in terms of the angle

6.2 Fastest climb

We analyzed solutions at various angles in order to determine the angle at which the duration of the climb is the shortest. In accordance with the results described in Section 6.1, the climbs were all performed with the largest possible initial speed. The fastest climbs were always obtained with this initial speed. Fig. 6 shows the duration of the climbs at various angles for the Silver Fox-like UAV and the Cessna 182. The Silver Fox like-UAV always started at its maximum speed of 66 m/s and the Cessna 182 at its maximum speed of 90 m/s. The fastest climb corresponds to the minimum in the curve of the duration of the climb in terms of the angle. These minimum can be clearly seen in the graphs of Fig. 6.

For the Silver Fox-like UAV, the fastest climb occurs at the angle of 31.2^0, at which angle, the airplane takes 99.2 s to reach 1800 m, with the final speed of 30.09 m/s. These parameters differ considerably from the textbooks parameters, which give the angle of 32.9^0 at the constant speed of 34.92 m/s. When actually solving the equation of motion with these textbook parameters, the climb obtained requires 126.4 s, which is much longer than the value we found for the actual fastest climb.

For the Cessna 182, the fastest climb occurs at the angle of 7.5^0; the airplane then takes 446.7 s to reach *2*700 m and its final speed is 33.76 m/s. As for the Silver Fox-like UAV, the values of these parameters for the fastest climb differ appreciably from the textbook values. Actually, the solution of the equation of motion with the textbook fastest climb angle of 9.57^0 and speed of 43.23 m/s, yield that the airplane stalls after 275.1 s, at the altitude of 1690.4 m.

6.3 Steepest climb

The steepest climb is the climb with the largest possible angle for which a solution of the equation of motion exists. The value of this angle can be seen in Fig. 6. For the Silver Fox-like UAV, this occurs at 41.9^0; at which angle the airplane takes 116.1 s to reach 1800 m, with the final speed of 15.18 m/s.

For the Cessna 182, the steepest climb occurs at 8.1^0; at which angle, the airplane takes *520.5* s to reach the altitude of 2800 m, with the final speed of 25.6 m/s.

Again, these parameters for the steepest climb differ from the standard values. For the Cessna 182, the solution of the equation of motion shows that, at the textbook optimal angle of 11.92^0 and

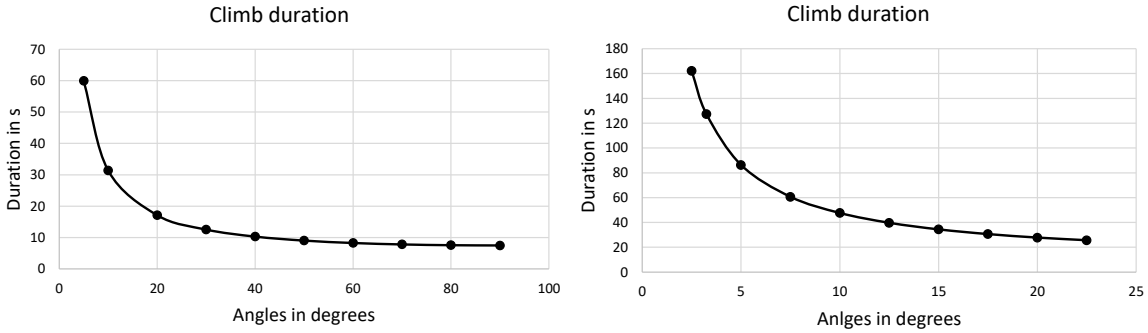

(a) For the Silver Fox-like UAV up to 300 m (b) For the Cessna 182 up to 500 m

Fig. 7 Climb duration at various angles

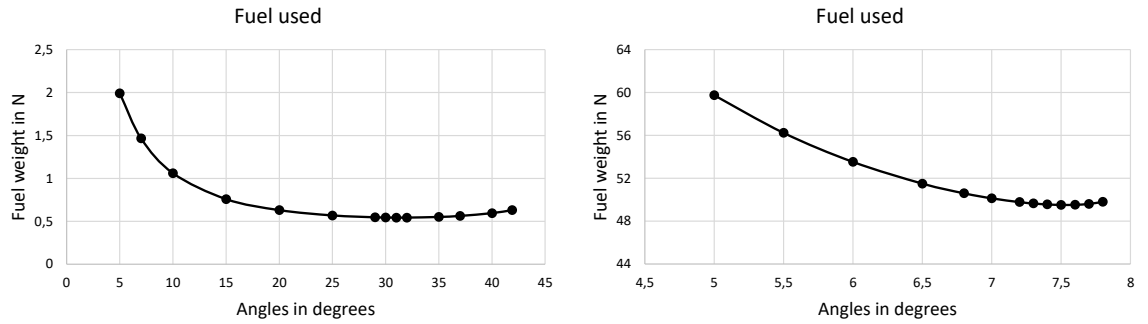

(a) For the Silver Fox-like UAV up to 1800 m (b) For the Cessna 182 up to 2700 m

Fig. 8 Amount of fuel in terms of the angle

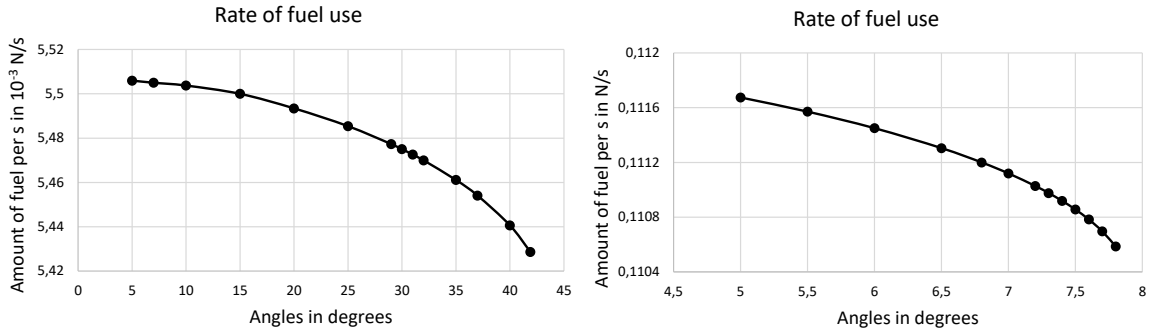

(a) For the Silver Fox-like UAV up to 1800 m (b) For the Cessna 182 up to 2700 m

Fig. 9 Rate of fuel use in climbs in terms of the angle

speed of 26.83 m/s, the airplane stalls after 55.3 s, at the altitude of 293.1 m.

It is noteworthy that for climbs to lower altitudes, there may not be a local minimum in the climb duration vs the angles, as was the case in Fig. 6. This is illustrated in Fig. 7 that shows the climb duration at various angles, for the Silver Fox-like UAV that climbs to 300 m and the Cessna 182 that climbs to 500 m. When there is no local minimum, the fastest climb is then also the steepest climb, because the minimum of the duration is at the largest angle possible.

For the Silver Fox-like UAV, the fastest climb to 300 m occurs at the angle of 90^0, and the

airplane then takes 7.5 s to reach this altitude. Its initial speed is 66 m/s and its final speed is 23.64 m/s.

For the Cessna 182, the fastest climb to 500 m occurs at 22.5^0, and the airplane takes 25.7 s to reach this altitude. Its initial speed is 90 m/s and its final speed is 22.90 m/s.

As is evident, for both airplanes, the speed is far from being constant and the parameters for the optimal flights differ appreciably from the value found in the textbooks for the optimal parameters.

6.4 Fuel consumption

The amount of fuel burned in the climbs is obtained by solving Eq. (18). Fig. 8 shows the amount of fuel required in the climbs at various angles, when the airplanes start at their maximum speeds. The amount of fuel used is seen to be minimum at the angle of the fastest climb.

Fig. 9 shows the rate of fuel burned in terms of the angle of climb. It is seen to decrease monotonically as the angle of inclination of the trajectory increases. It is minimum during the steepest climb.

Note that for Silver Fox-like UAV, these climbs require about 3% of its total amount of fuel, and for the Cessna 182, they require about 5% of its total fuel.

6.5 Speed, altitude, acceleration

Fig. 10 shows how the speed, the altitude and the acceleration vary in time during the steepest climb for the Silver Fox-like UAV. These variables also behave in the same way for the Cessna 182.

As can be seen in Fig. 10(a), the speed of the airplane decreases as it is climbing, and it reaches the prescribed altitude right at the instant at which its speed has decreased to its stall speed. This is a clear indication that, in this trajectory, the initial speed is the optimal speed for this climb. It starts with the largest speed the airplane can fly and any smaller initial speed will make the airplane stall before reaching the specified altitude.

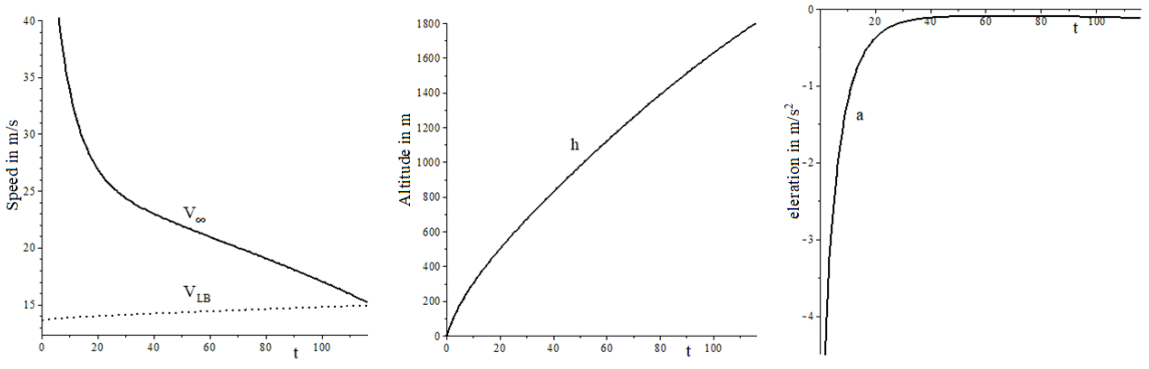

(a) Speed and stall speed (dotted) (b) Altitude (c) Acceleration

Fig. 10 Speed, altitude and acceleration as functions of t, for the Silver Fox-like UAV at full-power, from sea level up to 1800 m, with the optimal parameters for the steepest climb

The graph of the altitude as function of time, in Fig. 10(b) shows that it does not vary linearly; it has a definite curvature. Thus, a constant speed approximation may not be too appropriate for this motion. Fig. 10(c) shows that the airplane decelerates on the whole trajectory. Its acceleration changes very rapidly at first and it then becomes close to zero until the end of the trajectory.

Note that the behavior of these physical variables is very much the same in the fastest climbs.

7. Tables of maximum deceleration trajectories

In the process of trajectory construction, it is very helpful to be able to determine rapidly whether or not the airplane can go from a given speed V_1 to another one V_2, when flying on a trajectory inclined at an angle θ. In the present section, we give examples of tables that provide this information for the case when the airplane should decelerate as fast as possible. We will give similar tables for the maximum acceleration in the next section.

The following tables list, for different value of θ, the minimum possible speed V_f that can be reached when the airplane starts at its maximum speed. In these tables, the airplane starts on the ascending trajectories, from sea level, with its maximum speed and with its maximum weight, and flies until it reaches its stall speed or its ceiling. For the trajectory at 0^0, the duration, entered in the table, is the time required to reach a speed that is within 0.25 m/s of the "final" speed (this being defined here as its speed after 5000 s). All the descending trajectories start at the airplane ceiling h_c, which is 3700 m for the Silver Fox-like UAV and 5517 m for the Cessna 182, and terminate when the airplane reaches sea level.

The entries in the tables are at each 10^0 for the Silver Fox-like UAV and at each 2.5^0 for the Cessna 182. In the tables, V_i and V_f are respectively the initial and final speed on the trajectory, t_f is the duration of the trajectory, x_f is the horizontal distance covered. The angles that are marked with an asterisk correspond to trajectories that terminate when the airplane reaches its stall speed instead of its ceiling. The final altitude reached h_f can be calculated from the data in the table, as $h_f = h_i + x_f \tan(\theta)$. The deceleration from a speed V_1 to a speed V_2 will be possible if these two speeds are in the speed intervals $[V_i, V_f]$ shown in the tables. Note that these tables are simply given as examples; trajectories actually exist at any angle of inclination.

Table 2 Largest deceleration trajectories for the Silver Fox-like UAV

θ (deg.)	30*	20*	10*	0*	-10	-20	-30
V_i (m/s)	66.00	66.00	66.00	66.00	66.00	66.00	66.00
V_f (m/s)	14.82	15.42	15.76	15.80	45.86	65.86	80.30
t_f (s)	8.1	10.5	16.0	39.9	420.9	151.9	87.3
x_f (m)	269.0	379.1	593.6	1361.4	20983.7	10165.7	6408.6

Table 3 Largest deceleration trajectories for the Cessna 182

θ (deg.)	20*	15*	10*	5*	0*	-5	-10	-15	-20
V_i (m/s)	90	90	90	90	90	90	90	90	90
V_f (m/s)	22.72	23.01	23.20	23.26	23.13	49.00	81.18	101.71	118.60
t_f (s)	15.0	18.2	23.5	33.6	61.0	1096.1	345.9	191.5	128.7
x_f (m)	775.1	965.3	1261.7	1801.6	3172.8	63059.6	31288.5	20589.7	15157.8

Fig. 11(a) shows how the speed varies on the ascending trajectory at $\theta=10^0$ for the Cessna 182; the dotted line represents its approximation by the straight line described by the following equation:

$$V_{approx} = V_\infty(t_f) + m(t - t_f) \quad \text{with} \quad m = \frac{V_\infty(t_f) - V_\infty(0.5t_f)}{t_f - 0.5t_f}. \tag{21}$$

The corresponding approximation for the altitude $h_{approx}(t)$ is obtained by integrating Eq. (21). Fig. 11(b) shows the true altitude together with a dotted line that represents this approximation. Fig. 12 shows the same parameters for the Cessna 182 on a descending trajectory inclined at -10°. In both cases, the parabolic curves that represent $h_{approx}(t)$ can barely be discerned from the actual curve for $h(t)$. For both the ascending and the descending trajectories, it can be seen that these approximations are quite good, shortly after the departure. The same approximations can be made for the Silver Fox-like UAV.

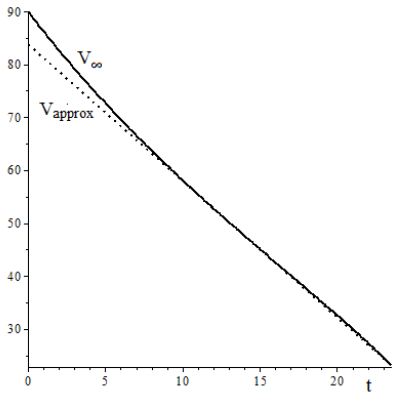

(a) Speed and its approximation (dotted)

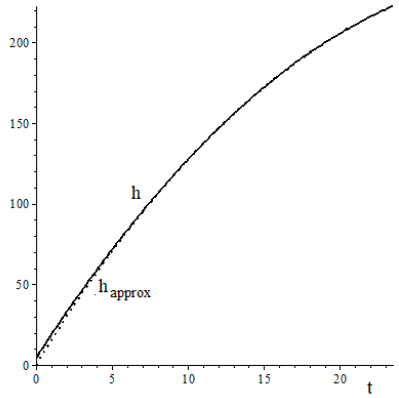

(b) Altitude and its approximation (dotted)

Fig. 11 Speed and altitude, with their approximations, for the Cessna 182 on the trajectory at 10^0

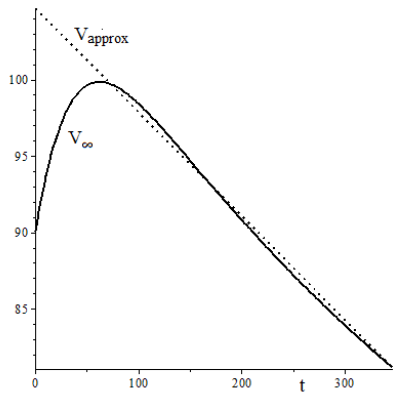

(a) Speed and its approximation (dotted)

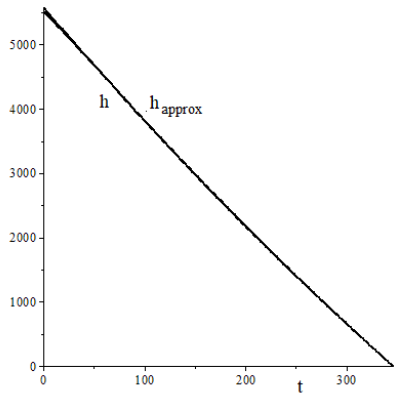

(b) Altitude and its approximation (dotted)

Fig. 12 Speed and altitude, with their approximations, for the Cessna 182 on the trajectory at -7.5^0

8. Tables of maximum acceleration trajectories

The following tables are similar to Tables 2 and 3. However in these trajectories, the airplane starts with its maximum weight and a speed that is just above its stall speed. These tables also give the amount of fuel required for the trajectory. Again, trajectories are possible at any angle of inclination, and the tables are just particular examples.

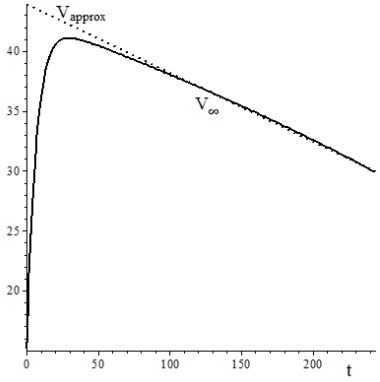

(a) Speed and its approximation (dotted)

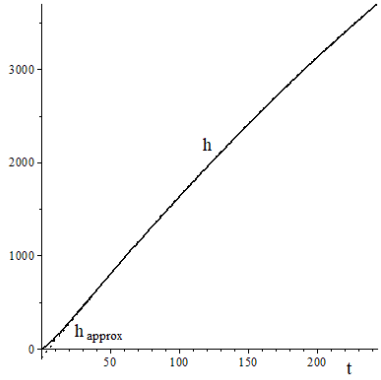

(b) Altitude and its approximation (dotted)

Fig. 13 Speed and altitude, with their approximations, for the Silver Fox-like UAV on the trajectory at 25^0

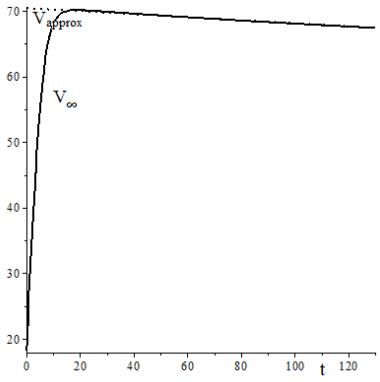

(a) Speed and its approximation (dotted)

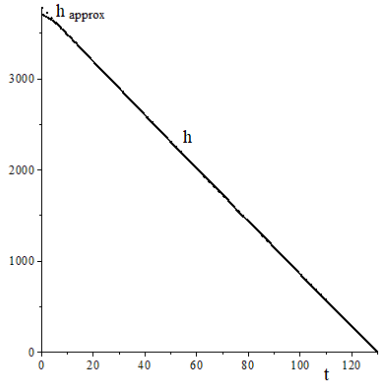

(b) Altitude and its approximation (dotted)

Fig. 14 Speed and altitude, with their approximations, for the Silver Fox-like UAV on the trajectory at -25^0

Table 4 Largest accelerations for the Silver Fox-like UAV

θ (deg)	35*	25	15	5	-5	-15	-25	-35
V_i (m/s)	14.40	15.14	15.63	15.87	19.08	18.78	18.20	17.31
V_f (m/s)	16.54	29.89	49.97	55.48	60.73	64.27	67.36	70.02
t_f (s)	204.6	243.6	299.2	760.1	698.6	222.2	130.0	92.4
x_f (m)	4200.4	7934.7	13808.6	42291.2	42291.2	13808.6	7934.7	5284.1
Fuel (N)	1.054	1.217	1.503	3.825	3.513	1.116	0.652	0.463

Table 5 Largest accelerations for the Cessna 182

θ (deg.)	7.5*	5*	2.5	0	-2.5	-5	-7.5	-10
V_i (m/s)	23.13	23.18	23.22	23.23	30.75	30.70	30.63	30.53
V_f (m/s)	26.58	29.12	54.89	76.37	83.61	91.04	98.37	105.54
t_f (s)	527.8	1043.5	2011.2	130*	1515.5	690.7	427.0	301.2
x_f (m)	22031.3	52572.8	1.26×10^5	8830.0	1.26×10^5	63059.6	41905.8	31288.5
Fuel (N)	58.29	105.5	196.1	16.6	148.4	67.5	41.6	29.3

Fig. 13(a) shows how the speed varies on the ascending trajectory at $\theta=25^0$ for the Silver Fox-like UAV; the dotted line represents its approximation by the straight line that corresponds to Eq. (21). Fig. 13(b) shows the altitude together with a dotted line corresponding to its approximation; the two curves are essentially undistinguishable. Fig. 14 shows the same parameters for a descending trajectory inclined at -25^0. Clearly, for both the ascending and the descending trajectories, these approximations are quite adequate, shortly after the departure. The corresponding approximations are also valid for the Cessna 182.

9. Conclusions

The automatic construction of airplane trajectories is usually done by concatenating elementary segments of trajectory called motion primitives. Most of these trajectories consist of straight lines that are connected by arcs of circles or helixes. A new observation is made in this article that states that it will, in fact, very rarely be possible to assemble complete trajectories with elementary segments of a common constant speed, as most authors propose doing. This motivated the present study of straight line segments on which the airplane decelerates or accelerates. In order to preserve as much as possible of the segments at constant speeds, we considered speeds that changed as fast as possible. That is, we looked at motion at the maximum decelerations and accelerations, i.e. at power-off and full power.

The article starts by recalling the equation of motion for an accelerating airplane on a rectilinear trajectory, which includes the variation of the air density and of the weight of the airplane due to fuel burn. We derived general formulas that express the constraints on the load factor, on the lift coefficient and on the power available for the motion.

We then reviewed the derivation found in textbooks of the conditions for optimal glides and climbs. Upon noting that only climbs at small inclination angles are usually considered, we produced a derivation of the corresponding conditions for any angle of inclination. This is a new result that completes the standard textbook presentations.

We point out shortcomings of the textbook presentations in that they wrongly consider that a limiting constant speed exists, and it neglects the change of the airplane weight as fuel is burned in climbing flights. The subsequent analysis that we present takes these facts into account. We determined the true value of the parameters for optimal glides and climbs, according to the actual solutions of the equation of motion.

We started by looking at gliding flights at power-off, for various angles of inclination and initial speeds. Upon plotting the glide durations for these different conditions, we obtained the value of the angle and the initial speed at which the glides are optimal. Our results show the

unexpected until now unknown features that

◦both the longest horizontal distance and the longest duration glides happen, in fact, at exactly the same angle and speed and

◦the angle and speed values given in textbooks, for both the longest distance and the longest duration glides, are incorrect by an appreciable amount. We give the true values.

We showed graphs of the speed, the altitude and the acceleration of the airplane as functions of time, in the optimal glides. These show very characteristic behaviors that had never been exhibited before.

We then analyzed the solutions of the equation of motion for climbs at full-power. By examining climbs durations at various speeds, we obtained the new result that the optimal climbs always occur when the initial speed is the maximum speed of the airplane. This is in contradistinction to what is found in all textbooks which always give two distinct speeds for the two optimal climbs which are actually not the maximum airplane speed.

By systematically varying the angle of inclination and plotting the glide durations at different angles, we obtained the value of the angle for the fastest climb, which corresponds to a minimum in the duration graph in terms of the angles. Our graphs also yield the value of the angle for the steepest climb, as the largest angle at which a solution exists. We obtained the unexpected results that

◦for climbs to higher altitudes the angles for the fastest and the steepest climbs differ, but they can take the same value for climbs to lower altitudes, as there is then no local minimum in the duration vs the angles curve,

◦the angle and speed values given in textbooks, for the fastest and the steepest climbs, are inaccurate by an appreciable amount. We give the true values.

We have solved the equation for the amount of fuel required for each full-power climb. We presented a graph of the solutions obtained, which yielded the new result that the minimum amount of fuel used occurs in the fastest climbs and the minimum rate of fuel burned occurs in the steepest climbs. For the Silver Fox-like UAV, these climbs require about 3% of its total amount of fuel, and for the Cessna 182, they require about 5% of its total fuel. These quantities should not be neglected, especially for trajectories that contain many climbing segments.

We showed graphs of the speed, the altitude and the acceleration of the airplane as functions of time, in the optimal climbs. These also show very characteristic behaviors that had never been exhibited before.

We produced sample tables that show, for various angles of inclination, the properties of the maximum decelerations. These tables exhibit the initial speed and the final speed attainable when the airplane is flying at power-off, the time it takes to decelerate from one speed to the other, and the horizontal distance covered in this process. Similar tables are shown for the possible maximum accelerations. They show the same parameters and also the amount of fuel required to accelerate from one speed to the other.

We proposed algebraic expressions to represent the speed, the altitude and the acceleration, which had never been done before. We show graphs that illustrate our approximation for the speed and the altitude superimposed with their true values. These indicate that our proposed approximation is quite good.

The results presented in this article are original in that they have never been published before. These results shed much light on what happens in flights at power-off and at full power and they

exhibit much fundamental information that was unknown until our work. They are very important for the automatic construction of UAV trajectories and they also constitute an important tool for the analysis of general airplane performances. Knowing how to optimize the range and duration in glides and climbs and the amount of fuel required can yield some worthwhile economy of operation of airplanes.

References

Aeronautics Learning Labratory for Science Technology and Research (ALLSTAR) of the Florida International University, (2011), *Propeller Aircraft Performance and The Bootstrap Approach*, http://www.allstar.fiu.edu/aero/BA-Background.htm.

Airliners.net (2015), http://www.airliners.net/aircraft-data/stats.main?id=145, Santa Monica, California, U.S.A.

Allaire, F., Tarbouchi, M. and Labonté, G. (2009), "FPGA implementation of genetic algorithm for UAV real-time path planning", *J. Intell. Robot. Syst.*, **54** (1-3), 495-510. https://doi.org/10.1007/978-1-4020-9137-7_26.

Ambrosino, G., Ariola, M., Ciniglio, U., Corraro, F., De Lellis, E. and Pironti, A. (2009), "Path generation and tracking in 3-D for UAVs", *IEEE T. Control Syst. Technol.*, **17**(4), 980-988. https://doi.org/10.1109/TCST.2009.2014359.

Anderson, J.D. Jr (2000), *Introduction to Flight*, Fourth Edition, *McGraw-Hill Series in Aeronautical and Aerospace Engineering*, Toronto, Canada.

Babaei, A.R. and Mortazavi, M. (2010), "Three-dimensional curvature-constrained trajectory planning based on in-flight waypoints", *J. Aircraft*, **47**(4), 1391-1398. https://doi.org/10.2514/1.47711.

Boschetti, P.J., Gonzalez, P. and Cardenas, E.M. (2015), "Program to calculate the performance of airplanes driven by a fixed-pitch propeller", *Proceedings of the AIAA Atmospheric Flight Mechanics Conference, AIAA SciTech Forum, (AIAA 2015-0015)*, Kissimmee, Florida, U.S.A., January.

Carpenter, P. (2018), RC Aerobatic Airplanes, RC Airplane World, https://www.rc-airplane-world.com/rc-aerobatic-airplanes.html

Cavcar, M. (2004), Propeller, School of Civil Aviation, Eskisehir, Turkey. https://fr.scribd.com/document/230664341/Propeller.

Chandler, P., Rasmussen, S. and Pachter, M. (2000), "UAV cooperative path planning", *Proceedings of the AIAA Guidance, Navigation, and Control Conference*, Denver, Colorado, U.S.A., August.

Chitsaz, H. and LaValle, S.M. (2007), "Time-optimal paths for a Dubins airplane", *Proceedings of the 46th IEEE Conference on Decision and Control*, New Orleans, Louisiana, U.S.A., December.

Commercial Aviation Safety Team (CAST), (2011), *Propeller Operation and Malfunctions Basic Familiarization for Flight Crews*, http://www.cast-safety.org/pdf/4_propeller_fundamentals.pdf.

Dubins, L.E. (1957), "On curves of minimal length with a constraint on average curvature and with prescribed initial and terminal positions and tangents", *Amer. J. Math.*, **79**, 497-516. https://doi.org/10.2307/2372560

Eshelby, M.E. (2000), *Aircraft Performance: Theory and Practice*, in *American Institute of Aeronautics and Astronautics Education Series*, Przemieniecki, J.S. Series Editor-in-Chief, AIAA, Inc., Reston, Virginia, U.S.A.

Filippone, A. (2006), *Flight Performance of Fixed and Rotary Wing Aircraft*, in *American Institute of Aeronautics and Astronautics Education Series*, Schetz, J.A. Series Editor-in-Chief, AIAA, Inc. and Butterworth-Heinemann, Herndon, Virginia, U.S.A.

Frazzoli, E., Dahleh, M.A. and Feron, E. (2005), "Maneuver-based motion planning for nonlinear systems with symmetries", *IEEE T. Robot.*, **21**(6), 1077-1091. https://doi.org/10.1109/TRO.2005.852260.

Gao, X.Z., Hou, Z.X., Zhu, X.F., Zhang, J.T. and Chen, X.Q. (2013), "The shortest path planning for manoeuvres of UAV", *Acta Polytechnica Hungarica,* **10**(1), 221-239.

Hale, F.J. (1984), *Introduction to Aircraft Performance, Selection*, and Design, John Wiley & Sons, New York, U.S.A.

Horizon Hobby (2017), https://www.horizonhobby.com/product/airplanes/airplane-accessories/airplane-engines-15042--1/gt80-twin-cylinder-(488-cu-in)-zene80t.

Hota, S and Ghose, D. (2010), "Optimal geometrical path in 3D with curvature constraint", *Proceedings of the IEEE/RSJ International Conference on Intelligent Robots and Systems (IROS)*, Taipei, Taiwan, October.

Hota, S. and Ghose, D. (2014), "Optimal trajectory planning for path convergence in three-dimensional space", *Proc. Inst. Mech. Eng. Part G J. Aerosp. Eng.*, **228**(5) 766-780. https://doi.org/10.1177%2F0954410013479714.

Hwangbo, M., Kuffner, J. and Kanade, T. (2007), "Efficient two-phase 3D motion planning for small fixed-wing UAVs", *Proceedings of the IEEE International Conference on Robotics and Automation*, Rome, Italy, April.

Jia, D. and Vagners, J. (2004), "Parallel evolutionary algorithms for UAV path planning", *Porceedings of the AIAA 1st Intelligent Systems Technical Conference*, Chicago, Illinois, U.S.A., September.

Jiabo, W., Li, L., Teng, L. and Zhu, W. (2012), "Three-dimensional constrained UAV path planning using modified particle swarm optimization with digital pheromones", *Proceedings of the EngOpt 2012- 3rd International Conference on Engineering Optimization*, Rio de Janeiro, Brazil, July.

Judd, K.B. (2001), "Trajectory planning strategies for unmanned air vehicles", Master Thesis, Brigham Young University, Provo, Utah, U.S.A.

Kok, K.Y. and Rajendran, P. (2016), "Differential evolution control parameter optimization for unmanned aerial vehicle path planning", *PLoS ONE*, **11**(3), https://doi.org/10.1371/journal.pone.0150558.

Labonté, G. (2012), "Formulas for the fuel of climbing propeller driven planes", *Aircraft Eng. Aerosp. Technol.*, **84**(1), 23-36. https://doi.org/10.1108/00022661211194951.

Labonté, G. (2015), "Simple formulas for the fuel of climbing propeller driven airplanes", *Adv. Aircraft Spacecraft Sci.*, **2**(4), 367-389. https://doi.org/10.12989/aas.2015.2.4.367.

Labonté, G. (2016), "Airplanes at constant speeds on inclined circular trajectories", *Adv. Aircraft Spacecraft Sci.*, **3**(4), 399-425. https://doi.org/10.12989/aas.2016.3.4.399.

Labonté, G. (2018), "On determining the flyability of airplane rectilinear trajectories at constant velocity", *Adv. Aircraft Spacecraft Sci.*, **5**(5), 551-579. https://doi.org/10.12989/aas.2018.5.5.551.

Mair, W.A and Birdsall, D.L. (1992), *Aircraft performance*, Cambridge University Press, Cambridge, U.K.

Maplesoft (2018), The Maple Software, https://www.maplesoft.com/contact/webforms/google/maple/MathSoftware.aspx?p=TC-5502&gclid=EAIaIQobChMIyqKc_oC93AIVB7bACh1wQgz7EAAYASAAEgLk2_D_BwE.

McIver, J. (2003), *Cessna Skyhawk II /100, Performance Assessment*, Temporal Images, Melbourne, Australia, http://www.temporal.com.au/c172.pdf.

Niendorf, M., Schmitt, F. and Adolf, F.M. (2013), "Multi-query path planning for an unmanned vixed-wing aircraft", *Proceedings of the AIAA Guidance, Navigation and Control (GNC) Conference*, Boston, Massachusetts, U.S.A., August.

Nikolos, I.K., Tsourveloudis, N.C. and Valavanis, K.P., (2003), "Evolutionary algorithm based 3-D path planner for UAV navigation", *IEEE T. Syst. Man Cybernet. Part B Cybernet.*, **33**(6), 898-912. https://doi.org/10.1109/TSMCB.2002.804370.

Parsch, A. (2006), "Silver Fox", Directory of U.S. Military Rockets and Missiles, Appendix 4, http://www.designation-systems.net/dusrm/app4/silverfox.html.

Phillips, W.F. (2004), *Mechanics of Flight*, John Wiley & Sons, Inc., Hoboken, New Jersey, U.S.A.

Ramana, M.V., Varma, S.A. and Kothari, M. (2016), "Motion planning for a fixed-wing UAV in urban environments", *Proceedings of the 4th IFAC Conference on Advances in Control and Optimization of Dynamical Systems ACODS 2016*, Tiruchirappalli, India, February.

Roberge, V., Tarbouchi, M. and Labonté, G (2012), "Comparison of parallel genetic algorithm and particle swarm optimization for real-time UAV path planning", *IEEE T. Industr. Inform.*, **9**(1), 132-141. https://doi.org/10.1109/TII.2012.2198665.

Roud, O. and Bruckert, D. (2006), *Cessna 182 Training Manual*, in *Red Sky Ventures and Memel CATS*, Second Edition 2011, Windhoek, Namibia.

Rudnick-Cohen, E., Azarm, S. and Herrmann, J.W. (2015), "Multi-objective design and path planning optimization of unmanned aerial vehicles (UAVs)", *Proceedings of the 16th AIAA/ISSMO Multidisciplinary Analysis and Optimization Conference*, Dallas, Texas, U.S.A., June.

Stengel, R.F. (2004), *Flight Dynamics*, Princeton University Press, Princeton, New Jersey, U.S.A.

Torenbeek, E. (1976), *Synthesis of Subsonic Airplane Design*, Delft University Press, Rotterdam, The Netherlands.

Wang, X., Jiang, P., Li, D. and Sun, T. (2017), "Curvature continuous and bounded path planning for fixed-wing UAVs", *Proceedings of the Sensors 2017*, Glasgow, Scotland, U.K., October-November.

Wang, Z., Liu, L., Long, T., Yu, C. and Kou, J. (2014), "Enhanced sparse A* search for UAV path planning using dubins path estimation", *Proceedings of the 33rd Chinese Control Conference (CCC)*, Nanjing, China, July.

Xia, L., Jun, X., Manyi, C., Ming, X. and Zhike, W. (2009), "Path planning for UAV based on improved A* algorithm", *Proceedings of the 9th International Conference on Electronic Measurement & Instruments, ICEMI '09*, Beijing, China, August.

Yang, K. and Sukkarieh, S. (2010), "An analytical continuous-curvature path-smoothing algorithm", *IEEE T. Robot*., **26**(3), 561-568. https://doi.org/10.1109/TRO.2010.2042990.

Yechout, T.R., Morris, S.L., Bossert, D.E. and Hallgren, W.F. (2003), *Introduction to Aircraft Flight Mechanics: Performance, Static Stability, Dynamic Stability, and Classical Feedback Control*, in *American Institute of Aeronautics and Astronautics Education Series*, Schetz, J.A. Series Editor-in-Chief, AIAA, Inc., Reston, Virginia, U.S.A.

Zhan, W., Wang, W., Chen, N. and Wang, C. (2014), "Efficient UAV path planning with multiconstraints in a 3D large battlefield environment", *Math. Probl. Eng*. http://dx.doi.org/10.1155/2014/597092.

Zheng, C., Ding, M. and Zhou, C. (2003), "Real-Time route planning for unmanned air vehicle with an evolutionary algorithm," *Int. J. Pattern Recog. Artif. Intell*., **17**(1), 63-81. https://doi.org/10.1142/S021800140300223X.

EC

Appendix A: Reference airplanes

We note that there could be small differences between the values we list here and the actual values for a particular model of the airplanes considered. We used values that we could find on the internet or estimate from the values for similar airplanes. These data are quite adequate for our purpose that is to illustrate the calculations involved in the formulas we have derived.

The thrust of the Cessna 182 is provided by a reciprocating engine with constant speed propeller; that of the Silver Fox by a reciprocating engine with a fixed pitch propeller. We recall that the efficiency of the propeller is a function of the advance ratio J, defined as:

$$J = \frac{V_\infty}{N\,D}$$

in which N is its number of revolution per second and D is its diameter. Thus the maximum power available P_{Amax} will depend on the speed, according to the equation:

$$P_{Amax} = \eta(J)P_{max}$$

The dependence of η on J for a constant speed propeller has the general features shown in Fig. 15(a). This curve approximates that given in Cavcar (2004) by the following quadratic expressions:

$$\eta(J) = \left[\frac{0.663}{0.640}\right]\left[J - 0.8\right]^2 + 0.8 \qquad \forall J \le 0.8.$$

$$\eta(J) = 0.8 \qquad \forall J > 0.8.$$

The dependence of η on J for a fixed pitch propeller has the general features shown in Fig. 15(b). This curve approximates that given in the Aeronautics Learning Laboratory for Science Technology and Research (ALLSTAR) of the Florida International University (2011) by the following quadratic expressions:

$$\eta(J) = -\left[\frac{0.83}{0.49}\right]\left[J - 0.70\right]^2 + 0.83 \quad \forall J \le 0.7.$$

$$\eta(J) = -\left[\frac{0.83}{0.06}\right]\left[J - 0.70\right]^2 + 0.83 \quad \forall J > 0.7.$$

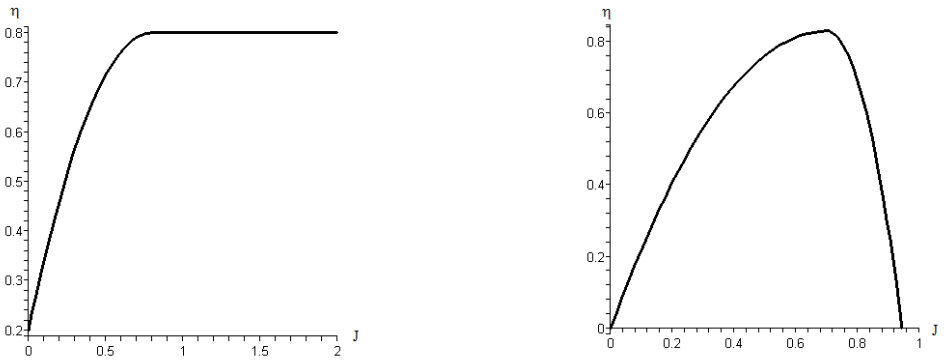

(a) Constant speed propeller (b) Constant pitch propeller

Fig. 15 Typical efficiency factor η as a function of the advance ratio J

Note that the propeller efficiency of this fixed pitch propellers goes to 0 at V_∞ = 66.1 m/s and becomes negative after that. Although a negative propeller efficiency might be desirable to slow down the airplane when it descends, it is not recommended to let this happens. When this happens, the propeller drives the engine and damage to the engine may result [see for example the Commercial Aviation Safety Team document (2011). We shall therefore not allow speeds larger than that value.

A.1 Cessna 182 Skylane

The parameters listed are W_1 = the weight of the empty airplane, W_0 = the maximum take-off weight, W_F = the maximum weight of fuel, b = the wingspan, S = the wing area, e = Oswald's efficiency factor, C_{Lmax} = the maximum global lift coefficient, C_{D0} = the global drag coefficient at zero lift, n_{max} and n_{min} are respectively the maximum and minimum value of the load factor, P_{Pmax} = maximum breaking power at sea level, RPM = number of revolution per minute, Diameter = diameter of the propeller, η_{max} = maximum value of the propeller efficiency.

The characteristic parameters for the Cessna 182 can be found in Airliners.net (2015), Roud and Bruckert (2006) and McIver (2003). Some of the parameters, which were not readily available, were estimated from those of the very similar Cessna 172.

A.2 Silver Fox-like UAV

The Silver Fox UAV is presently produced by Raytheon. Some of its specifications can be found in Parsch (2006). The power available $P_A(0)$ for the Silver Fox is only about 370 W, which allows it to climb only at low angles. Meanwhile, it is common for Radio Controlled (RC) airplanes to climb at very steep angles (See for example Carpenter (2018)). Thus, upon taking advantage of motors that have been developed in this domain, a Silver Fox-like airplane could be endowed with much more power in order to improve considerably its manoeuvre envelope. One such motor is the Zenoah GT-80 Twin Cylinder 80cc (ZENE80T). It weighs 34 N and outputs 4045 W at 7500 rpm. (Horizon Hobby 2017). We shall consider a Silver Fox-like UAV with such a motor.

Table 6 Characteristic parameters of the Cessna 182

W_1 = 7,562 N	W_0 = 11,121 N	W_F =1737 N
b = 11.02 m	S = 16.1653 m^2	e = 0.75
C_{Lmax} = 2.10	C_{D0} = 0.029	n_{max} = 3.8, n_{min} = -1.52
P_{Pmax} = 171.511 kW	RPM = 2,600	
Const. speed propeller	Diameter = 2.08 m	η_{max} = 0.80

Table 7 Characteristic parameters of the Silver Fox-Like airplane

W_1 = 100.0 N	W_0 = 148.0 N	W_F = 19.1 N
b = 2.4 m	S = 0.768 m^2	e = 0.8
C_{Lmax} = 1.26	C_{D0} = 0. 0251	n_{max} = 5.0, n_{min} = -2.0
P_{Pmax} = 4.413 kW	RPM = 7500	c = 7.4475×10^{-7}
Fixed pitch propeller	Diameter = 0.56 m	η_{max} = 0.77
h_c = 3700 m		